

LA-UR-21-23193 (Accepted Manuscript)

Oxygen Ion Dynamics in the Earth's Ring Current: Van Allen Probes Observations

Yue, Chao; Bortnik, Jacob; Li, Wen; Ma, Qianli; Wang, C. P.; Thorne, Richard M.; Lyons, Larry; Reeves, Edmond Geoffrey David; Spence, H. E.; Gerrard, Andrew J.; Gkioulidou, M.; Mitchell, Donald G.

Provided by the author(s) and the Los Alamos National Laboratory (2021-11-19).

To be published in: Journal of Geophysical Research: Space Physics

DOI to publisher's version: 10.1029/2019JA026801

Permalink to record: <http://permalink.lanl.gov/object/view?what=info:lanl-repo/lareport/LA-UR-21-23193>

Disclaimer:

Los Alamos National Laboratory, an affirmative action/equal opportunity employer, is operated by Triad National Security, LLC for the National Nuclear Security Administration of U.S. Department of Energy under contract 89233218CNA000001. By approving this article, the publisher recognizes that the U.S. Government retains nonexclusive, royalty-free license to publish or reproduce the published form of this contribution, or to allow others to do so, for U.S. Government purposes. Los Alamos National Laboratory requests that the publisher identify this article as work performed under the auspices of the U.S. Department of Energy. Los Alamos National Laboratory strongly supports academic freedom and a researcher's right to publish; as an institution, however, the Laboratory does not endorse the viewpoint of a publication or guarantee its technical correctness.

Yue Chao (Orcid ID: 0000-0001-9720-5210)
Bortnik Jacob (Orcid ID: 0000-0001-8811-8836)
Li Wen (Orcid ID: 0000-0003-3495-4550)
Ma Qianli (Orcid ID: 0000-0001-5452-4756)
Wang Chih-Ping (Orcid ID: 0000-0003-2393-6808)
Thorne Richard, Mansergh (Orcid ID: 0000-0003-2410-3437)
Lyons Larry, R. (Orcid ID: 0000-0002-9867-3638)
Spence Harlan, E. (Orcid ID: 0000-0002-2526-2205)
Gerrard Andrew, J. (Orcid ID: 0000-0002-9626-2085)
Gkioulidou Matina (Orcid ID: 0000-0001-9979-2164)
Mitchell Donald, G. (Orcid ID: 0000-0003-1960-2119)

Oxygen Ion Dynamics in the Earth's Ring Current: Van Allen Probes

Observations

Chao Yue¹, Jacob Bortnik¹, Wen Li², Qianli Ma^{1,2}, Chih-Ping Wang¹, Richard M. Thorne¹, Larry Lyons¹, Geoffrey D. Reeves^{3,4}, Harlan E. Spence⁵, Andrew J. Gerrard⁶, Matina Gkioulidou⁷, and Donald G. Mitchell⁷

1. Department of Atmospheric and Oceanic Sciences, UCLA, Los Angeles, CA, USA.
2. Center for Space Physics, Boston University, Boston, MA, USA
3. Space Science and Applications Group, Los Alamos National Laboratory, Los Alamos, NM, USA.
4. Space Sciences Division at the New Mexico Consortium, Los Alamos, NM, USA.
5. Institute for the Study of Earth, Oceans, and Space, University of New Hampshire, Durham, New Hampshire, USA.
6. Center for Solar-Terrestrial Research at New Jersey Institute of Technology, New Jersey, USA
7. Johns Hopkins University Applied Physics Laboratory, Laurel, Maryland, USA

This is the author manuscript accepted for publication and has undergone full peer review but has not been through the copyediting, typesetting, pagination and proofreading process, which may lead to differences between this version and the [Version of Record](#). Please cite this article as doi: [10.1029/2019JA026801](https://doi.org/10.1029/2019JA026801)

Abstract

Oxygen (O^+) enhancements in the inner magnetosphere are often observed during geomagnetically active times, such as geomagnetic storms. In this study, we quantitatively examine the difference in ring current dynamics with and without a substantial O^+ ion population based on almost 6 years of Van Allen Probes observations. Our results have not only confirmed previous finding of the role of O^+ ions to the ring current but also found that abundant O^+ ions are always present during large storms when $\text{sym-H} < -60$ nT without exception, whilst having the pressure ratio (\mathcal{R}) between O^+ and proton (H^+) larger than 0.8 and occasionally even larger than 1 when $L < 3$. Simultaneously, the pressure anisotropy decreases with decreasing sym-H and increasing L shell. The pressure anisotropy decrease during the storm main phase is likely related to the pitch angle isotropization processes. In addition, we find that \mathcal{R} increases during the storm main phase and then decreases during the storm recovery phase, suggesting faster buildup and decay of O^+ pressure compared to H^+ ions, which are probably associated

with some species dependent source and/or energization as well as loss processes in the inner magnetosphere.

Plain Language Summary: The behavior of the ionospheric O^+ ions in the Earth's ring current should be carefully examined in order to advance our understanding of the role of ion composition in ring current dynamics. This problem has been extensively studied using past spacecraft missions. In this study, we revisit this problem based on almost 6 years of high-quality data from the Van Allen Probes and have confirmed previous finding about the role of O^+ ions to the ring current. For example, more O^+ ions contribute to the ring current as sym-H decreases, and O^+ and total plasma pressures dramatically build up during storm time. Besides, our statistical results also provide evidence that without exception, ionospheric O^+ ions make a significant contribution to the ring current during active time and their relative contribution to the ring current increases during the storm main phase and then decreases during the storm recovery phase compared to those of H^+ ions, suggesting a faster buildup and decay of O^+ pressure. In addition, the decrease of pressure anisotropy during the storm main phase is related to the pitch angle isotropization, which is probably caused by current sheet scattering or wave-particle interaction.

Key Points:

1. We quantitatively examine how the total plasma pressure and pressure anisotropy changes with and without a substantial O^+ ion population
2. O^+ ions always make a non-negligible contribution to the ring current when $\text{sym-H} < -60$ nT with $\mathcal{R} > 0.8$
3. The decrease of pressure anisotropy during storm main phase is related to pitch angle isotropization.

1. Introduction

The Earth's ring current, located at an equatorial distance between 2 and 7 R_E , is greatly intensified during geomagnetic storms when convection is strongly enhanced for a prolonged period (> a few hours). The main carriers of the ring current are ions of various species, including light protons (H^+) and heavy oxygen ions (O^+) with energies ranging from one to a few hundred keV [Williams, 1985; Gkioulidou *et al.*, 2016; Yue *et al.*, 2018; Keika *et al.*, 2018a]. These ions are injected from the Earth's plasma sheet

and/or have direct access into the inner magnetosphere from the terrestrial ionosphere [e.g., *Delcourt et al.*, 1992; *Sheldon et al.*, 1998; *Huddleston et al.* 2005; *Chappell et al.*, 1987; 2000; 2008; *Kronberg et al.*, 2014; *Keika et al.*, 2016; 2018b; *Gkioulidou et al.*, 2019]. As geomagnetic activity increases, a greater variety of ion species are transported into the inner magnetosphere including the heavier O^+ ions, forming a stronger ring current. During the transport process, these ions get energized through adiabatic transport associated with large-scale convection and/or with mesoscale impulsive dipolarizations, as well as localized nonadiabatic acceleration [e.g., *Yang et al.*, 2011; *Zong et al.*, 2012; *Zhou et al.*, 2012; *Keika et al.*, 2013]. The dominant energization processes affecting ring current ions are still under investigation. When the geomagnetic activity diminishes, these ions (especially O^+) are lost due to Coulomb collisions and charge exchange processes with the geocorona [e.g., *Fok et al.*, 1991; *Daglis et al.*, 1999] as well as pitch angle scattering by electromagnetic ion cyclotron (EMIC) waves [e.g., *Kennel and Petschek*, 1966; *Jordanova et al.*, 1997; *Meredith et al.*, 2003; *Jordanova*, 2007] and/or current sheet scattering [e.g., *Sergeev and Tsyganenko*, 1982; *Sergeev et al.* 1983; 1993; *Donovan et al.*, 2003; *Yue et al.*, 2014; *Liang et al.*, 2014]. As a result, the ions are removed and the ring current decays back to quiescent levels.

The quiescent ring current is carried mainly by protons (H^+) of predominantly solar wind origin, while both in situ observations and modeling work [e.g., *Gloeckler et al.*, 1985; *Krimigis et al.*, 1985; *Hamilton et al.*, 1988; *Daglis and Axford*, 1996; *Daglis*

et al., 1999; *Fu et al.*, 2001; *Liu*, 2003; *Fok et al.*, 2001; 2006; 2011; *Denton et al.*, 2005; *Ebihara et al.*, 2006; *Ohtani et al.*, 2006; *Yue et al.*, 2011; *Kistler et al.*, 2016; *Claudepierre et al.*, 2016] have confirmed that singly charged O^+ ions originating from the Earth's ionosphere make a significant contribution to the plasma pressure in the Earth's inner magnetosphere during active times. This compositional change can affect several dynamical processes, such as species- and energy- dependent transport and charge exchange, wave excitation and propagation, as well as pitch angle scattering loss [e.g., *Fok et al.*, 1991; *Summers et al.*, 2007].

Measurements of O^+ abundance provide an important clue regarding ring current dynamics during both geomagnetically quiet and active times. A number of studies have described the O^+ dynamics by using various observations at different locations [e.g., *Mitchell et al.*, 2003; *Gloeckler et al.*, 1985; *Kronberg et al.*, 2015; *Kistler and Mouikis*, 2016], but only a few comprehensive statistical analyses have been performed to investigate the O^+ dynamics near the equator inside $L < 7$ during active times, where the ring current is predominately located [e.g., *Keika et al.* 2016; *Kistler et al.*, 2016; *Fernandes, et al.*, 2017; *Valek et al.*, 2018]. This deficiency was largely due to the lack of sufficient in situ O^+ measurements near the magnetic equator in the inner magnetosphere with high time resolution, wide energy coverage, and broad spatial coverage.

A systematic investigation of the O^+ ion behavior is critical in order to advance our understanding of plasma dynamics and wave activities, such as the source and loss

processes in the Earth's inner magnetosphere as geomagnetic activity changes. In this study, we perform a statistical survey to revisit the question of O^+ ion contribution to the ring current plasma pressure using almost 6 years of high-quality Van Allen Probes data, from October 2012 to September 2018. We quantitatively examine how the total plasma pressure and pressure anisotropy change with and without an abundant O^+ ion population.

2. Dataset and methodology

The Van Allen Probes (RBSP) mission, which consists of two identically instrumented spacecraft (probes A and B), orbits near the equator (10° inclination) with a perigee at $\sim 1.1 R_E$ and an apogee at $\sim 5.8 R_E$ [Mauk *et al.*, 2013] and a period of ~ 9 hrs. Both satellites are equipped with comprehensive suites of particles and fields measurement instrumentation. Here we perform our statistical analysis by using the most recent level-3 unidirectional differential flux measurements from the Helium, Oxygen, Proton, and Electron (HOPE) Mass Spectrometer [Funsten *et al.*, 2013] of the Energetic Particle Composition and Thermal Plasma (ECT) Suite [Spence *et al.*, 2013] and the Radiation Belt Storm Probes Ion Composition Experiment (RBSPICE) [Mitchell *et al.*, 2013] instrument onboard Van Allen Probes (both A and B). The combined measurements from both instruments cover the H^+ , O^+ , helium (He^+) and electron (e^-) energies from several eV to several hundreds of keV.

We use the 1-min time resolution unidirectional fluxes to calculate the plasma pressures of four different species in the parallel ($P_{\parallel,i}$) and perpendicular ($P_{\perp,i}$) directions as well as the total plasma pressure and pressure anisotropy, where subscript “ i ” represents the species, i.e., H^+ , O^+ , He^+ and electrons. The partial plasma pressure (P_i) of different species is $P_i = (2 P_{\perp,i} + P_{\parallel,i})/3$ and the total plasma pressure (P_t) is the sum of partial plasma pressures from different species including H^+ , O^+ , He^+ and electrons. The pressure anisotropy is $A = \frac{P_{\perp}}{P_{\parallel}}$, where P_{\parallel} and P_{\perp} are the pressures in parallel and perpendicular directions to the background magnetic field, respectively. More details about the data processing and pressure calculation could be found in our previous study [Yue *et al.*, 2018]. Although we neglected the 50-140 keV O^+ channels from the RBSPICE instrument because of contamination [e.g., Yue *et al.*, 2018], we adjusted the energy boundary between the highest HOPE and lowest RBSPICE energy channels so that the pressure integration covers all energies from 1 eV to 1 MeV. The accuracy of this approach is demonstrated in S9 in Supporting Information (SI) in Yue *et al.* [2018].

In this study, we have included the Van Allen Probe observational data from October 2012 to September 2018, which covers half of the current solar cycle with solar maximum in 2014 and approaching solar minimum in 2019. The plasma pressure amplitudes and variation trends are similar during geomagnetic storms of similar

intensity in different years with different F10.7 values, indicating that the solar cycle effect should be small in our ring current pressure investigation. Only the data points with $P_H > 0.5$ nPa, $P_O > 0.1$ nPa and magnetic local time (MLT) from noon to midnight are used (> 2.8 million data points) in our statistics to ensure that they are taken in the dominant ring current region to exclude the effects of asymmetry, and are substantially above the noise level. Here we separate the data into two categories to investigate how O^+ behavior may affect the inner magnetospheric plasma dynamics: (1) The O^+ pressure is a significant component of the total plasma pressure, indicated by having the pressure ratio of O^+ to H^+ ($\mathcal{R} = P_O/P_H$) > 0.35 ; (2) the O^+ pressure is a minor component of total plasma pressure, with $\mathcal{R} < 0.15$. These criteria are chosen to include a sufficient, and roughly similar numbers of data in each category to ensure statistical significance (i.e., 25% of the data points are in category 1 where $\mathcal{R} > 0.35$ and 28% in category 2 where $\mathcal{R} < 0.15$) and to have a clear separation boundary between these two distinct situations. It should be noted that the median values are used for our statistical results throughout the paper, since the distribution would not be fully characterized by the mean and the standard deviation alone if the distribution is not a normal one.

3. Results

In this section, we present the Van Allen Probe observations by first showing a typical storm time event that occurred from 05 to 09 March 2016, and then following up

with a statistical survey. The case study provides an overview of where the Van Allen Probe measurements are taken and how the plasma pressure and pressure anisotropy vary as function of L shell and geomagnetic activity to better assist our understanding of the statistical results.

3.1 Case study

Figure 1 illustrates the plasma pressure and pressure anisotropy variations during the storm event from 05 to 09 March 2016 observed by Van Allen Probe A with an apogee near the dawn sector (Figure 1f). Figures 1a-1c show the solar wind interplanetary magnetic field (IMF) B_z (black line in 1a), the solar wind dynamic pressure (red line in 1a), geomagnetic AE index (1b) and sym-H index (1c). It is shown in Figure 1c that this is a double dip storm event with sym-H minimum values of ~ -100 nT around 21 UT on March 6 and around 5 UT on March 7. During the storm main phase from 15 UT on March 6 to 5 UT on March 7, the IMF was mainly southward (Figure 1a, black line) and the solar wind dynamic pressure (Figure 1a, red line) was high above 8 nPa, while AE (Figure 1b) reached over 1400 nT. Figure 1d shows the plasma pressure variation observed for the total plasma pressure (P , black), H^+ pressure (P_H , blue), and O^+ pressure (P_O , red). It can be seen that the total plasma pressure is mainly contributed by the H^+ ions throughout the storm, except the period around the sym-H minimum when the O^+ pressure increases dramatically from less than 0.5 nPa to 5 nPa near apogee (a factor of ~ 10 increase). The O^+ pressure builds up rapidly during the storm main phase and

gradually decays as sym-H recovers. In addition, the pressure anisotropy $A = \frac{P_{\perp}}{P_{\parallel}}$ (Figure 1e) decreases during the storm main phase but remains >1 most of the time, and it then gradually increases during the storm recovery phase.

In order to better visualize the spatiotemporal variations of pressure and anisotropy, Figures 1g to 1j show the total pressure, H^+ and O^+ pressures, as well as anisotropy variation as a function of L shell during four different time intervals enclosed by the vertical lines with different colors in Figures 1a-1f. These time intervals are all chosen during Van Allen probe A outbound passes, with very similar magnetic latitude (MLAT) ranges (Figure 1f) to reduce the variations of pressure and pressure anisotropy due to the orbital effects. The four time intervals represent the different storm phases as labeled in the legend of Figure 1h. From the pre-storm time (black line) to storm main phase (red line), the H^+ , O^+ and total pressures increase dramatically, with the total plasma pressure at $L=4$ increasing from 3 to 20 nPa (a factor of ~ 7 increase) and O^+ pressure from 0.1 to 10 nPa (a factor of ~ 100 increase), while the pressure anisotropy decreases from 2.2 to about 1.2. The pressure anisotropy increases with decreasing L shell in general which is mainly caused by betatron acceleration and the pre-storm distribution matches well with the quiet time pressure anisotropy profile from *Lui et al.* [1994], demonstrating that this case study is representative. From the storm main phase (red line) to post-storm time (blue line), the O^+ and total pressures (Figures 1g and 1i) decrease at all L shells but the decrease is more evident at low L shells, with the peak

location moving to higher L shells as sym-H increases, indicating stronger losses at the lower L shells which may be potentially caused by charge exchange and Coulomb collisions that predominantly occur at lower L shells [Fok *et al.*, 1991]. Meanwhile, the pressure anisotropy gradually increases from the main phase to the post-storm time.

3.2 Statistical results

The case presented above demonstrates the strong variations of ion pressures and pressure anisotropy during storm time at different L shells. In order to better visualize how O^+ ions evolve under different geomagnetic conditions at different locations, Figure 2 shows the statistical distributions of plasma pressures and pressure anisotropy variation as functions of sym-H and L shell in the two categories that we define in section 2: $\mathcal{R} > 0.35$ (Figures 2a-2f) and $\mathcal{R} < 0.15$ (Figures 2g-2l). The panels shown in Figure 2 from top to bottom are: the satellite cumulative time spent in the particular L and sym-H bin with $P_o > 0.1$ nPa, $P_H > 0.5$ nPa and outside the dawn sector with $MLT=3-9$ under the conditions $\mathcal{R} > 0.35$ (Figures 2a-2f) and $\mathcal{R} < 0.15$ (Figures 2g-2l); the “probability”, which is defined as the ratio of the satellite cumulative time under the condition of $\mathcal{R} > 0.35$ or $\mathcal{R} < 0.15$ (shown in Figure 2a or 2g) relative to the total cumulative time without any \mathcal{R} limitation; the median values of the O^+ pressure (Figure 2c and 2i); the total pressure (Figure 2d and 2j); the pressure anisotropy (Figure 2e and 2k); and the pressure ratio \mathcal{R} (Figure 2f and 2l). It is shown in Figure 2b that the probability of observing $\mathcal{R} >$

0.35 events is much higher when sym-H is lower, especially when sym-H < -60 nT that the probability is higher than 80% at all L shells and the ratio \mathcal{R} itself is larger than 0.8 and even larger than 1 at L < 3 (Figure 2f). This suggests that without exception, O⁺ ions make a significant contribution ($\mathcal{R} > 0.8$) to the ring current when sym-H < -60 nT. On the other hand, the probability without much O⁺ ($\mathcal{R} < 0.15$) is zero at most L shells when sym-H is less than -60 nT (Figure 2h). In addition, there is strong correlation between the probability and \mathcal{R} when sym-H is above -60 nT in Figure 2h and 2l, the higher the probability, the lower of the value \mathcal{R} and the high probability region is limited at sym-H > -30 nT and L < 5. All these observational features suggest that O⁺ ions are always absent during relatively quiet condition, in other words, it further confirms that O⁺ ions are involved when sym-H is strongly negative (< -60 nT) and no storm events exist without O⁺ ions being present. Moreover, compared with the situation of $\mathcal{R} < 0.15$ (Figures 2i-2j), the O⁺ pressure and total plasma pressure are much larger and the pressure peak moves to low L shells as sym-H decreases (Figures 2c and 2d) which is consistent with previous studies [e.g., *Krimigis et al.*, 1985; *Greenspan and Hamilton*, 2002; *Fu et al.*, 2001]. Meanwhile, the anisotropy in Figure 2e is much smaller than that in Figure 2k but larger than 1, and the anisotropy decreases with decreasing sym-H and increasing L shell. The anisotropy decreasing with increasing L shell is consistent with the main cause being due to betatron acceleration [*Cowley and Ashour-Abdalla*,1975; *Southwood and Kivelson*, 1975].

The statistical results shown in Figure 2 imply that O^+ ions are always involved during storm time, and that the abundance of O^+ ions becomes larger as the storm becomes stronger. In order to investigate statistically the temporal evolution of the ring current with abundant O^+ ions during storm time, we have binned all the data points with $\mathcal{R} > 0.35$ and $P_o > 0.1$ nPa, $P_H > 0.5$ nPa into a time frame of 12 hrs before to 36 hrs after the local sym-H minimum (S_0). To establish this relative time frame, for each data point at time t_i , we search the sym-H index in the interval from t_i-36 hrs to t_i+12 hrs and identify the local sym-H minimum (S_0), which occurs at some time t_0 . The epoch time $t=t_i-t_0=0$ represents the observation time t_i that is at the local sym-H minimum S_0 , while $t < 0$ means that the observation data point is collected before the local minimum of sym-H or during storm main phase, and $t > 0$ means that the observation data point is collected after the local sym-H minimum or during storm recovery phase.

The results of the superposed epoch analysis with $S_0 < -30$ nT and $3 < L < 5$ (roughly the main region of the ring current) and outside $MLT= 3-9$ are shown in Figure 3. The blue and red lines with 25% and 75% quartiles represent the situations of -70 nT $< S_0 < -30$ nT and $S_0 < -70$ nT, respectively. The x-axis is the time difference ($t= t_i-t_0$) between the observational point (t_i) and the local minimum sym-H (t_0). Figures 3a–3d show the satellite cumulative time, sym-H, IMF Bz and AE index, respectively. It is shown that sym-H minimizes at $t=0$ with a median value around -40 nT (blue line) and -80 nT (red line) in Figure 3b, representing weak storms and moderate storms,

respectively. Meanwhile, IMF Bz (Figure 3c) decreases during the storm main phase with minimum values of -4 nT (blue line) and -9 nT (red line) around $t = 0$, and then increases to zero during most of the time of the storm recovery; AE index (Figure 3d) increases during storm main phase and peaks around 500 nT (blue line) and 700 nT (red line) at $t = 0$ and then decreases during the recovery phase. These temporal evolutions of IMF Bz and AE index suggest strong energy loading and unloading processes during storm main phase and recovery phase.

In addition, the O^+ and total plasma pressures increase at $t < 0$, peak around $t = 0$, and then gradually decay during storm recovery as shown in Figures 3e and 3f. Compared with weak storms (blue line), the pressures are larger and variations are stronger for moderate storms (red line). While these variations are expected during storm time [e.g., *Smith and Hoffman, 1973; Hamilton et al. 1989; Zhao et al., 2015*], it is interesting to find that \mathcal{R} (Figure 3h) increases substantially during the main phase of moderate storms (red line) and becomes largest with a median value of 0.9 around $t = 0$ and then rapidly decays at $t > 0$, suggesting that O^+ ion buildup and decay rates are much faster than H^+ ions. Moreover, the pressure anisotropy decreases at $t < 0$ and gradually increases at $t > 0$ (Figure 3g), which is consistent with our previous case study shown in Figure 1.

To investigate further why the pressure anisotropy decreases during the storm main phase and increases during storm recovery phase, we have plotted in Figure 4 the

superposed epoch analysis with $S_o < -30$ nT, $3 < L < 5$ and MLT from noon to midnight of the normalized flux of several different energies (from less than 1 keV to 100s keV) as a function of pitch angle (PA) and epoch time for H^+ (Figure 4a and 4b) and O^+ (Figure 4c and 4d) during weak (-70 nT $< S_o < -30$ nT) (Figure 4a and 4c) and moderate ($S_o < -70$ nT) (Figure 4b and 4d) storms to demonstrate the PA evolution. The normalized flux at each PA bin is obtained from the statistical result of median number flux divided by the flux averaged over all the pitch angle bins at that specific epoch time. It is shown that the previous pancake distributions (i.e., having peaks around 90°) of the 5 and 50 keV H^+ ions become more isotropic distribution near $t = 0$ during weak storms (Figure 4a), and the higher energy (100 and 400 keV) H^+ also show isotropic distributions around $t = 0$ during moderate storms (Figure 4b). Similar results are seen in O^+ PA distributions (Figure 4c and 4d). These observations suggest that pressure anisotropy decreases during storm main phase is most likely related to the PA isotropization.

4. Discussion and Conclusions

In this study, we have quantitatively examined the O^+ ion dynamics that contribute to the ring current variation in the inner magnetosphere, based on almost 6 years of Van Allen Probes observations. The results presented in this study have largely confirmed previous findings about the role of O^+ ions in the ring current dynamics by using previous spacecraft missions [e.g., *Smith and Hoffman, 1973; Krimigis et al., 1985;*

Hamilton et al., 1988; Fu et al., 2001; Greenspan and Hamilton, 2002]. For example, more O^+ ions always appear in the ring current during active times and the O^+ and total plasma pressures dramatically build up during the storm main phase and peak around the sym-H minimum. They then gradually decay during the storm recovery phase with O^+ pressure decaying significantly faster than the total pressure.

In addition, the statistical results also provide evidence that low O^+ contribution ($\mathcal{R} < 0.15$) only occurs when sym-H > -60 nT, indicating that O^+ ions seldom appear in the ring current during relatively quiet or moderate geomagnetic conditions. On the other hand, O^+ ions (without exception) make a significant contribution to the ring current when sym-H < -60 nT (probability $> 80\%$ with $\mathcal{R} > 0.35$ and \mathcal{R} itself is > 0.8 in Figure 2f). The larger contribution of ionospheric O^+ to the ring current may be related to the stronger substorm activity during storm times (stronger southward IMF B_z and higher AE values are shown in Figures 3c and 3d during stronger storm main phase). The generation of field-aligned currents and particle precipitation during substorms [*McPherron et al., 1968; Hasegawa and Sato, 1979; Liu et al., 2015; Yue et al., 2015*] initiate more H^+ and O^+ outflows through the field-aligned currents [e.g., *Welling et al., 2015; Zou et al., 2017*] that are then energized during transport from the tail plasma sheet to the inner magnetosphere and contribute to the storm time ring current.

These O^+ and H^+ ions either enter directly into the ring current from the ionosphere at $L < \sim 5$, or enter the tail plasma sheet first at much higher L-shells and are

then transported earthward and energized through conservation of the first two adiabatic invariants [e.g., *Huddleston et al.* 2005; *Chappell et al.*, 1987; 2000; 2008]. In our study, we have found that the pressure anisotropy decreases while both perpendicular and parallel pressures increase during the storm main phase, which means that there are stronger pressure variations in the parallel direction than those in the perpendicular direction. These observations suggest the possible direct access of ionospheric H^+ and O^+ ions into the ring current or an isotropization process (e.g., current sheet scattering and pitch angle scattering by EMIC waves) that would transfer ion pressure preferentially from the perpendicular to the parallel direction during active times. Based on energetic H^+ and O^+ PA distributions, we have found that the anisotropy decreases during storm main phase is related to PA isotropization. As the ring current builds up significantly during the storm main phase, the magnetic field lines become more stretched, which may lead to stronger energy-dependent current sheet scattering, especially for heavier O^+ ions that have larger gyro-radii [e.g., *Sergeev and Tsyganenko*, 1982; *Sergeev et al.* 1983; 1993; *Yue et al.*, 2014]. This scattering helps isotropize the ion PADs and thus the pressure anisotropy decreases. During storm recovery phase as the ring current gradually decays and magnetic field lines becomes less stretched, the scattering effect weakens. In addition, pitch angle scattering caused by EMIC waves may also reduce the pressure anisotropy. However, the EMIC waves are not considered to be the dominant mechanism since they are MLT-dependent and wave occurrence rates are generally small [e.g.,

Saikin et al., 2015; 2016; *Zhang et al.*, 2016; *Jun et al.*, 2019; *Yue et al.*, 2019]. In addition, the anisotropy increases during storm recovery phase. This may indicate stronger loss processes in the field-aligned direction than in the perpendicular direction, possibly due to strong charge exchange and coulomb collisions, which predominantly occur in the parallel direction during the storm recovery phase [e.g., *Fok et al.*, 1995; *Jordanova et al.*, 1996].

As shown in Figure 3, the pressure ratio between the O^+ and H^+ increases during the storm main phase and decreases during the storm recovery phase, suggesting that O^+ ions buildup and decay rates are much faster than H^+ ions. The faster buildup of O^+ ions is probably related with some species dependent source and/or energization processes in the inner magnetosphere [*Daglis et al.*, 1999; *Sheldon et al.*, 1998]. On the other hand, the faster decay of O^+ ions may be caused by their stronger charge exchange and Coulomb collision rate [*Fok et al.*, 1991]. Here, we have estimated the decay rates of O^+ and H^+ by fitting the observed O^+ and H^+ pressure profiles during storm recovery phase using an exponential decay function $f(t)=f_0*e^{(-\tau t)}$. The decay rates of O^+ are 0.02/hr (lifetime of 50 hrs) for weak storms and 0.03/hr (lifetime of 33 hrs) for moderate storms, and it is 0.012/hr (lifetime of 83 hrs) for H^+ both during weak and moderate storms, indicating that O^+ loss processes depend on magnetic activity which may be different from H^+ loss processes.

Based on the work done by *Smith and Bewtra* [1978], we have also calculated the decay rates of O^+ and H^+ due to charge exchange. We assume that the neutral Hydrogen density is about $100/\text{cm}^3$ at $L = 4$ near the geomagnetic equator. Here we choose 10s keV H^+ and O^+ to calculate their charge exchange lifetimes since they are the main population of ring current. For O^+ of 25 and 64 keV, the calculated lifetimes are 100 hrs and 55 hrs, respectively, and for H^+ of 38 and 48 keV, the lifetimes are 55 hrs and 83 hrs, respectively. The observed H^+ lifetime during the storm recovery phase is similar to the charge exchange estimation, suggesting that charge exchange may be the dominant loss process for H^+ ions. On the other hand, the charge exchange lifetimes of 10s keV O^+ are much longer than the observed ones that also depend on the geomagnetic activity, suggesting that, in addition to charge exchange, other loss processes such as Coulomb decay and pitch angle scattering may also play important roles in O^+ loss during the storm recovery phase.

In conclusion, we perform a statistical survey to revisit the question of the O^+ ion contribution to the ring current plasma pressure. We have found that:

- (1) Consistent with previous studies, more O^+ ions contribute to the ring current as sym-H decreases, and O^+ and total plasma pressures dramatically build up during the storm main phase and peak around the sym-H minimum. They then gradually decay during the storm recovery phase with O^+ pressure decaying significantly faster than the total pressure.

- (2) The probability of high pressure ratios of O^+ to H^+ (i.e., $\mathcal{R} > 0.8$) increases to $>80\%$ when $\text{sym-H} < -60$ nT. On the other hand, the possibility of $\mathcal{R} < 0.15$ is zero as $\text{sym-H} < -60$ nT. These observations indicate that O^+ ions always make a significant contribution ($\mathcal{R} > 0.8$) to the ring current when $\text{sym-H} < -60$ nT without exception.
- (3) The pressure ratio of O^+ to H^+ increases during storm main phase and then rapidly decays during storm recovery phase, suggesting that O^+ ion buildup and decay rates are much faster than H^+ ions. The faster buildup of O^+ ions is probably related to some species-dependent source and/or energization processes in the inner magnetosphere. On the other hand, the faster decay of O^+ ions may be caused by the stronger charge exchange and Coulomb collision rates.
- (4) The pressure anisotropy decreases with decreasing sym-H and increasing L . The fact that anisotropy decreases during storm main phase and then gradually increases during storm recovery phase suggests that there are stronger pressure variations in the parallel direction than that in the perpendicular direction during storm time. Based on the energetic H^+ and O^+ PA distributions, the anisotropy decreases during storm main phase is likely related to the PA isotropization process.

Acknowledgments

This work was supported by the NASA LWS grant NNX14AN85G and NASA HTIDeS NNX16AG21G. WL would like to acknowledge the NASA grants NNX15AI96G and

Author Manuscript

NNX17AG07G, and Alfred P. Sloan Research Fellowship (FG-2018-10936). We acknowledge use of Van Allen Probes data of the Level 3 HOPE uni-dimensional particle flux data obtained from the RBSP-ECT website (https://rbsp-ect.lanl.gov/data_pub/rbspa/hope/level3/pitchangle/), made publicly available through NASA prime contract number NAS5-01072; the Level 3 RBSPICE uni-dimensional particle flux data obtained from the RBSPICE website (http://rbspicea.ftecs.com/Level_3PAP/); the Level 3 magnetometer data obtained from the RBSP EMFISIS website (emfisis.physics.uiowa.edu/Flight/RBSP-B/L3). We thank the Space Physics Data Facility at the NASA Goddard Space Flight Center for providing the OMNI data (<https://cdaweb.gsfc.nasa.gov/index.html/>).

References:

Chappell, C.R., Moore, T.E., Waite Jr, J.H. (1987). The ionosphere as a fully adequate source of plasma for the Earth's magnetosphere. *Journal of Geophysical Research* 92, 5896.

Chappell, C. R., Giles, B. L., Moore, T. E., Delcourt, D. C., Craven, P. D., & Chandler, M. O. (2000). The adequacy of the ionospheric source in supplying magnetospheric plasma. *Journal of Atmospheric and Solar-Terrestrial Physics*, 62(6), 421-436.

Chappell, C. R., M. M. Huddleston, T. E. Moore, B. L. Giles, and D. C. Delcourt (2008), Observations of the warm plasma cloak and an explanation of its formation in the magnetosphere, *J. Geophys. Res.*, 113, A09206, doi:10.1029/2007JA012945.

Claudepierre, S. G., Chen, M. W., Roeder, J. L., & Fennell, J. F. (2016). An empirical model of ion plasma in the inner magnetosphere derived from CRRES/MICS measurements. *Journal of Geophysical Research: Space Physics*, 121, 11,780–11,797. <https://doi.org/10.1002/2016JA023468>

Daglis, L. A., R. M. Thorne, W. Baumjohann, and S. Orsini (1999), The terrestrial ring current: Origin, formation, and decay, *Rev. Geophys.*, 37(4), 407–438.

Daglis, I. A., & Axford, W. I. (1996). Fast ionospheric response to enhanced activity in geospace: Ion feeding of the inner magnetotail. *Journal of Geophysical Research: Space Physics*, 101(A3), 5047-5065.

De Michelis, P., I. A. Daglis, and G. Consolini (1999), An average image of proton plasma pressure and of current systems in the equatorial plane derived from AMPTE/CCE-CHEM measurements, *J. Geophys. Res.*, 104(A12), 28615–28624, doi:10.1029/1999JA900310.

Denton, M. H., M. F. Thomsen, H. Korth, S. Lynch, J. C. Zhang, and M. W. Liemohn (2005), Bulk plasma properties at geosynchronous orbit, *J. Geophys. Res.*, 110, A07223, doi:10.1029/2004JA010861.

Donovan, E. F., Jackel, B., Strangeway, R., & Klumpar, D. (2003). Energy dependence of the latitude of the 1–25 KeV ion isotropy boundary. *Sodankylä Geophysical Observatory Publications*, 92, 11-14.

Ebihara, Y., M. Yamada, S. Watanabe, and M. Ejiri (2006), Fate of outflowing suprathermal oxygen ions that originate in the polar ionosphere, *J. Geophys. Res.*, 111, A04219, doi:10.1029/2005JA011403.

Fernandes, P. A., et al. (2017), The plasma environment inside geostationary orbit: A Van Allen Probes HOPE survey, *J. Geophys. Res. Space Physics*, 122, 9207-9227, doi:10.1002/2017JA024160.

Fok, M.-C., R. A. Wolf, R. W. Spiro, and T. E. Moore (2001), Comprehensive computational model of Earth's ring current, *J. Geophys. Res.*, 106(A5), 8417–8424, doi:10.1029/2000JA000235.

Fok, M. - C., T. E. Moore, P. C. Brandt, D. C. Delcourt, S. P. Slinker, and J. A. Fedder (2006), Impulsive enhancements of oxygen ions during substorms, *J. Geophys. Res.*, 111, A10222, doi:10.1029/2006JA011839.

Fok, M.-C., T. E. Moore, S. P. Slinker, J. A. Fedder, D. C. Delcourt, M. Nosé, and S.-H. Chen (2011), Modeling the superstorm in November 2003, *J. Geophys. Res.*, 116, A00J17, doi:10.1029/2010JA015720.

Fok, M. - C., J. U. Kozyra, A. F. Nagy, and T. E. Cravens (1991), Lifetime of ring current particles due to coulomb collisions in the plasmasphere, *J. Geophys. Res.*, 96(A5), 7861-7867, doi: 10.1029/90JA02620.

Fok, M. C., Moore, T. E., Kozyra, J. U., Ho, G. C., & Hamilton, D. C. (1995). Three dimensional ring current decay model. *Journal of Geophysical Research: Space Physics*, 100(A6), 9619-9632.

Fu, S. Y., Wilken, B., Zong, Q. G., & Pu, Z. Y. (2001). Ion composition variations in the inner magnetosphere: Individual and collective storm effects in 1991. *Journal of Geophysical Research: Space Physics*, 106(A12), 29683-29704.

Funsten, H. O. et al. (2013), Helium, Oxygen, Proton, and Electron (HOPE) Mass Spectrometer for the Radiation Belt Storm Probes Mission, *Space Sci Rev*, 1–62, doi:10.1007/s11214-013- 9968-7.

Gkioulidou, M., A. Y. Ukhorskiy, D. G. Mitchell, and L. J. Lanzerotti (2016), Storm time dynamics of ring current protons: Implications for the long-term energy budget in the inner magnetosphere, *Geophys. Res. Lett.*, 43, doi:10.1002/2016GL068013.

Gkioulidou, M., Ohtani, S., Ukhorskiy, A. Y., Mitchell, D. G., Takahashi, K., Spence, H. E., et al (2019). Low energy (< keV) O⁺ outflow directly into the inner magnetosphere: Van Allen Probes Observations. *Journal of Geophysical Research: Space Physics*, 124. <https://doi.org/10.1029/2018JA025862>

Gloeckler, G., Wilken, B., Stüdemann, W., Ipavich, F. M., Hovestadt, D., Hamilton, D. C., & Kremser, G. (1985). First composition measurement of the bulk of the storm-time ring current (1 to 300 keV/e) with AMPTE-CCE. *Geophysical Research Letters*, 12(5), 325–328. <https://doi.org/10.1029/GL012i005p00325>

Greenspan, M. E., & Hamilton, D. C. (2002). Relative contributions of H⁺ and O⁺ to the ring current energy near magnetic storm maximum. *Journal of Geophysical Research: Space Physics*, 107(A4).

Hamilton, D. C., G. Gloeckler, F. M. Ipavich, W. Stüdemann, B. Wilken, and G. Kremser (1988), Ring current development during the great geomagnetic storm of February 1986, *J. Geophys. Res.*, 93, 14,343–14,355.

Hasegawa, A., & Sato, T. (1979). Generation of field aligned current during substorm. In *Dynamics of the Magnetosphere* (pp. 529-542). Springer, Dordrecht.

Huddleston, M. M., C. R. Chappell, D. C. Delcourt, T. E. Moore, B. L. Giles, and M. O. Chandler (2005), An examination of the process and magnitude of ionospheric plasma supply to the magnetosphere, *J. Geophys. Res.*, 110, A12202, doi:10.1029/2004JA010401.

Jordanova, V. K. (2007), Modeling geomagnetic storm dynamics: New results and challenges, *J. Atmos. Sol. Terr. Phys.*, 69, 56–66, doi:10.1016/j.jastp.2006.06.016.

Jordanova, V. K., J. U. Kozyra, A. F. Nagy, and G. V. Khazanov (1997), Kinetic model of the ring current - atmosphere interactions, *J. Geophys. Res.*, 102, 14,279–14,291, doi:10.1029/96JA03699.

Jordanova, V. K., Kistler, L. M., Kozyra, J. U., Khazanov, G. V., & Nagy, A. F. (1996). Collisional losses of ring current ions. *Journal of Geophysical Research: Space Physics*, 101(A1), 111-126.

Jun, C. - W., C. Yue, J. Bortnik, L.R. Lyons, Y.T. Nishimura, C.A. Kletzing, J. Wygant, and H.E. Spence. (2019), A statistical study of EMIC waves associated with and without energetic particle injection from the magnetotail, *J. Geophys. Res. Space Physics*, 124. <https://doi.org/10.1029/2018JA025886>

Keika, K., Kistler, L. M., & Brandt, P. C. (2013). Energization of O⁺ ions in the Earth's inner magnetosphere and the effects on ring current buildup: A review of previous observations and possible mechanisms. *Journal of Geophysical Research: Space Physics*, 118, 4441–4464. <https://doi.org/10.1002/jgra.50371>

Keika, K., Seki, K., Nosé, M., Machida, S., Miyoshi, Y., Lanzerotti, L.J., Mitchell, D.G., Gkioulidou, M., Turner, D., Spence, H. and Larsen, B.A., (2016). Storm time impulsive enhancements of energetic oxygen due to adiabatic acceleration of preexisting warm oxygen in the inner magnetosphere. *Journal of Geophysical Research: Space Physics*, 121(8), pp.7739-7752.

Keika, K., Kasahara, S., Yokota, S., Hoshino, M., Seki, K., Nosé, M., et al. (2018a). Ion energies dominating energy density in the inner magnetosphere: Spatial distributions and composition, observed by Arase/MEP - i. *Geophysical Research Letters*, 45, 12,153–12,162. <https://doi.org/10.1029/2018GL080047>

Keika, K., Seki, K., Nosé, M., Miyoshi, Y., Lanzerotti, L. J., Mitchell, D. G., Gkioulidou, M., & Manweiler, J. W. (2018b). Three-step buildup of the 17 March 2015 storm ring current: Implication for the cause of the unexpected storm intensification. *Journal of Geophysical Research: Space Physics*, 123. <https://doi.org/10.1002/2017JA024462>

Kennel, C. F., and H. E. Petschek (1966), Limit on stably trapped particle fluxes, *J. Geophys. Res.*, 71, 1–28. ^[1]_[SEP]

Kistler, L. M., and C. G. Mouikis (2016), The inner magnetosphere ion composition and local time distribution over a solar cycle, *J. Geophys. Res. Space Physics*, 121, 2009–2032, doi:10.1002/2015JA021883.

Kistler, L.M., Mouikis, C.G., Spence, H.E., Menz, A.M., Skoug, R.M., Funsten, H.O., Larsen, B.A., Mitchell, D.G., Gkioulidou, M., Wygant, J.R. and Lanzerotti, L.J., (2016). The source of O⁺ in the storm time ring current. *Journal of Geophysical Research: Space Physics*, 121(6), pp.5333-5349.

Krimigis, S. M., G. Gloeckler, R. W. McEntire, T. A. Potemra, F. L. Scarf, and E. G. Shelley (1985), Magnetic storm of September 4, 1984: A synthesis of ring current

spectra and energy densities measured with AMPTE/ CCE, *J. Geophys. Res.*, 12(5), 329–332.

Kronberg, E. A., Ashour-Abdalla, M., Dandouras, I., Delcourt, D. C., Grigorenko, E. E., Kistler, L. M., et al. (2014). Circulation of heavy ions and their dynamical effects in the magnetosphere: Recent observations and models. *Space Science Reviews*, 184(1–4), 173–235. <https://doi.org/10.1007/s11214-014-0104-0>

Kronberg, E. A., E. E. Grigorenko, S. E. Haaland, P. W. Daly, D. C. Delcourt, H. Luo, L. M. Kistler, and I. Dandouras (2015), Distribution of energetic oxygen and hydrogen in the near-Earth plasma sheet, *J. Geophys. Res. Space Physics*, 120, 3415–3431, doi:10.1002/2014JA020882.

Liang, J., E. Donovan, B. Ni, C. Yue, F. Jiang, and V. Angelopoulos (2014), On an energy - latitude dispersion pattern of ion precipitation potentially associated with magnetospheric EMIC waves, *J. Geophys. Res. Space Physics*, 119, 8137–8160, doi:10.1002/2014JA020226.

Liu, J., V. Angelopoulos, X. Chu, X. Zhou, and C. Yue (2015), Substorm current wedge composition by wedgelets. *Geophys. Res. Lett.*, 42, 1669–1676. doi:10.1002/2015GL063289.

Lui, A. T. Y. (2003), Inner magnetospheric plasma pressure distribution and its local time asymmetry, *Geophys. Res. Lett.*, 30(16), 1846, doi:10.1029/2003GL017596.

Mauk, B. H., N. J. Fox, S. G. Kanekal, R. L. Kessel, D. G. Sibeck, and A. Ukhorskiy (2013), Science Objectives and Rationale for the Radiation Belt Storm Probes Mission, *Space Sci Rev*, 179(1), 3–27, doi:10.1007/s11214-012-9908-y.

McPherron, R. L., Parks, G. K., Coroniti, F. V., & Ward, S. H. (1968). Studies of the magnetospheric substorm: 2. Correlated magnetic micropulsations and electron precipitation occurring during auroral substorms. *Journal of Geophysical Research*, 73(5), 1697-1713.

Meredith, N., R. Thorne, R. Horne, D. Summers, B. Fraser, and R. Anderson (2003), Statistical analysis of relativistic electron energies for cyclotron resonance with EMIC waves observed on CRRES, *J. Geophys. Res.*, 108(A6), 1250, doi:10.1029/2002JA009700

Mitchell, D., C:Son-Brandt, P., Roelof, E., Hamilton, D., Retterer, K., & Mende, S. (2003). Global imaging of O⁺ from IMAGE/HENA. *Space Science Reviews*, 109, 63–75. <https://doi.org/10.1023/B:SPAC.0000007513.55076.00>

Mitchell, D. G., et al. (2013), Radiation Belt Storm Probes Ion Composition Experiment (RBSPICE), *Space Sci. Rev.*, 179, doi:10.1007/s11214-013-9995-4.

Ohtani, S., P. C. Brandt, H. J. Singer, D. G. Mitchell, and E. C. Roelof (2006), Statistical characteristics of hydrogen and oxygen ENA emission from the storm-time ring current, *J. Geophys. Res.*, 111, A06209, doi:10.1029/2005JA011201.

Saikin, A. A., J.-C. Zhang, R. C. Allen, C. W. Smith, L. M. Kistler, H. E. Spence, R. B. Torbert, C. A. Kletzing, and V. K. Jordanova (2015), The occurrence and wave properties of H⁺, He⁺, and O⁺-band EMIC waves observed by the Van Allen Probes, *J. Geophys. Res. Space Physics*, 120, 7477–7492, doi:10.1002/2015JA021358.

Saikin, A. A., Zhang, J. C., Smith, C. W., Spence, H. E., Torbert, R. B., & Kletzing, C. A. (2016). The dependence on geomagnetic conditions and solar wind dynamic pressure of the spatial distributions of EMIC waves observed by the Van Allen Probes. *Journal of Geophysical Research: Space Physics*, 121(5), 4362-4377.

Sergeev, V. A., and N. A. Tsyganenko (1982), Energetic particle losses and trapping boundaries as deduced from calculations with a realistic magnetic field model, *Planet. Space Sci.*, 10, 999.

Sergeev V. A., Sazhina, E. M., Tsyganenko, N. A., Lunblad, J. A., and Soraas F (1983). Pitch angle scattering of energetic protons in the magnetotail current sheet as the dominant source of their isotropic precipitation into the nightside ionosphere, *Planet Space Sci.*, 31, 1147–1158.

Sergeev, V. A., Malkov, M., & Mursula, K. (1993). Testing the isotropic boundary algorithm method to evaluate the magnetic field configuration in the tail. *Journal of geophysical research*, 98(A5), 7609-7620.

Smith, P. H., and R. A. Hoffman (1973), Ring current particle distributions during the magnetic storms of December 16-18, 1971, *J. Geophys. Res.*, 78(2), 4731-, doi:10.1029/JA078i022p04731.

Smith, P. H., & Bewtra, N. K. (1978). Charge exchange lifetimes for ring current ions. *Space Science Reviews*, 22(3), 301-318.

Spence, H.E., Reeves, G.D., Baker, D.N., Blake, J.B., Bolton, M., Bourdarie, S., Chan, A.A., Claudepierre, S.G., Clemmons, J.H., Cravens, J.P. and Elkington, S.R., (2013). Science goals and overview of the radiation belt storm probes (RBSP) energetic particle, composition, and thermal plasma (ECT) suite on NASA's Van Allen probes mission. *Space Science Reviews*, 179(1-4), pp.311-336.

Summers, D., B. Ni, and N. P. Meredith (2007), Timescales for radiation belt electron acceleration and loss due to resonant wave - particle interactions: 2. Evaluation for VLF chorus, ELF hiss, and electromagnetic ion cyclotron waves, *J. Geophys. Res.*, 112, A04207, doi: 10.1029/2006JA011993.

Valek, P. W., Delmonico, E., McComas, D. J., Goldstein, J., Allegrini, F., & Livi, S. (2018). Composition of 1–128 keV magnetospheric ENAs. *Journal of Geophysical Research: Space Physics*, 123. <https://doi.org/10.1002/2017JA024997>

Welling, D. T., V. K. Jordanova, A. Gloer, G. Toth, M. W. Liemohn, and D. R. Weimer (2015), The two-way relationship between ionospheric outflow and the ring current, *J. Geophys. Res. Space Physics*, 120, 4338–4353, doi:10.1002/2015JA021231.

Williams, D. J. (1985), 'Dynamic of the Earth's Ring Current: Theory and Observation', *Space Sci. Rev.* 42, 375–396.

Yang, B., Zong, Q.G., Wang, Y.F., Fu, S.Y., Song, P., Fu, H.S., Korth, A., Tian, T. and Reme, H., (2010). Cluster observations of simultaneous resonant interactions of ULF waves with energetic electrons and thermal ion species in the inner magnetosphere. *Journal of Geophysical Research: Space Physics*, 115(A2).

Yue, C., Q. Zong, Y. Wang, I. I. Vogiatzis, Z. Pu, S. Fu, and Q. Shi (2011), Inner magnetosphere plasma characteristics in response to interplanetary shock impacts, *J. Geophys. Res.*, 116, A11206, doi:10.1029/2011JA016736.

Yue, C., C. - P. Wang, L. Lyons, J. Liang, E. F. Donovan, S. G. Zaharia, and M. Henderson (2014), Current sheet scattering and ion isotropic boundary under 3 - D empirical force - balanced magnetic field, *J. Geophys. Res. Space Physics*, 119, 8202-8211, doi:10.1002/2014JA020172.

Yue, C., C. - P. Wang, Y. Nishimura, K. R. Murphy, X. Xing, L. Lyons, M. Henderson, V. Angelopoulos, A. T. Y. Lui, and T. Nagai (2015), Empirical modeling of 3 - D force - balanced plasma and magnetic field structures during substorm growth phase, *J. Geophys. Res. Space Physics*, 120, 6496–6513, doi: 10.1002/2015JA021226.


Yue, C., Bortnik, J., Li, W., Ma, Q., Gkioulidou, M., Reeves, G. D., et al. (2018). The composition of plasma inside geostationary orbit based on Van Allen Probes observations.

Journal of Geophysical Research: Space Physics, 123, 6478–6493.

<https://doi.org/10.1029/2018JA025344>

Yue, C., Jun, C. - W., Bortnik, J., An, X., Ma, Q., Reeves, G. D., et al. (2019). The relationship between EMIC wave properties and proton distributions based on Van Allen probes observations. *Geophysical Research Letters*, 46. <https://doi.org/10.1029/2019GL082633>

Zhang, X.J., Li, W., Thorne, R.M., Angelopoulos, V., Bortnik, J., Kletzing, C.A., Kurth, W.S. and Hospodarsky, G.B., (2016). Statistical distribution of EMIC wave spectra: Observations from Van Allen Probes. *Geophysical Research Letters*, 43(24).

Zhao, H., X. Li, D. N. Baker, J. F. Fennell, J. B. Blake, B. A. Larsen, R. M. Skoug, H. O. Funsten, R. H. W. Friedel, G. D. Reeves H. E. Spence, D. G. Mitchell, L. J. Lanzerotti, J. V. Rodriguez (2015), The evolution of ring current ion energy density and energy content during geomagnetic storms based on Van Allen Probes measurements, *J. Geophys. Res. Space Physics*, 120, 7493–7511, doi:10.1002/2015JA021533. 

Zhou, X.Z., Ge, Y.S., Angelopoulos, V., Runov, A., Liang, J., Xing, X., Raeder, J. and Zong, Q.G., (2012). Dipolarization fronts and associated auroral activities: 2. Acceleration of ions and their subsequent behavior. *Journal of Geophysical Research: Space Physics*, 117(A10).

Zong, Q. G., Wang, Y. F., Zhang, H., Fu, S. Y., Wang, C. R., Yuan, C. J., & Vogiatzis, I. (2012). Fast acceleration of inner magnetospheric hydrogen and oxygen ions by shock induced ULF waves. *Journal of Geophysical Research: Space Physics*, 117(A11).

Zou, S., A. Ridley, X. Jia, E. Boyd, M. Nicolls, A. Coster, E. Thomas, and J. M. Ruohoniemi (2017), PFISR observation of intense ion upflow fluxes associated with an SED during the 1 June 2013 geomagnetic storm, *J. Geophys. Res. Space Physics*, 122, 2589–2604, doi:10.1002/2016JA023697.

Figure Captions:

Figure 1. The Van Allen Probe A observation of a storm event from 05 to 09 March 2016. (a) IMF B_z component (black) and solar wind dynamic pressure (red); (b) AE index; (c) sym-H index; (d) H^+ (blue), O^+ (red) and total (black) plasma pressures; (e) total pressure anisotropy; (f) the L shell (black) and MLT (red) of satellite trajectory. The vertical dashed lines mark the outbound pass time intervals represent the pre-storm (black), storm main phase (red), recovery phase (green) and the post-storm time (blue). Panel (g) – (j) show total plasma pressure, anisotropy, proton pressure and oxygen pressure distributions as a function of L shell during these four time intervals to demonstrate the storm time dynamics.

Figure 2. The statistical distributions of O^+ and total plasma pressures as functions of sym-H and L shells under two levels of pressure ratio between O^+ and H^+ : (a-f) $P_o/P_H > 0.35$ and (g-l) $P_o/P_H < 0.15$ with the condition of $P_H > 0.5$ nPa and $P_o > 0.1$ nPa and MLT from noon to midnight to ensure that the oxygen and total plasma pressures are significantly above the noise level and to make sure the measurements are taken in the dominant ring current region. The panels from top to bottom are (a and g) the satellite cumulative time with $P_o > 0.1$ nPa and $P_H > 0.5$ nPa under the condition of $\mathcal{R} > 0.35$ and outside MLT=3-9 (Figure 2a) or $\mathcal{R} < 0.15$ (Figure 2g), (b and h) “probability” which is defined as the ratio of satellite cumulative time under the condition of $\mathcal{R} > 0.35$ or $\mathcal{R} < 0.15$ (shown in Figure 2a or Figure 2g) relative to the total cumulative time without any \mathcal{R} limitation with $P_o > 0.1$ nPa and $P_H > 0.5$ nPa and outside MLT = 3-9, (c and i) the median values of O^+ pressure, (d and j) total plasma pressure, (e and k) pressure anisotropy and (f and l) \mathcal{R} .

Figure 3. The temporal evolution of pressure and anisotropy as a function of time difference ($t=t_i - t_0$) between the observational point (t_i) and the universal time (t_0) of local sym-H minimum (S_o) in the time window of 12 hours before and 36 hours after the time t_0 . Only the data points of $\mathcal{R} > 0.35$ and $P_H > 0.5$ nPa and $P_o > 0.1$ nPa with $S_o < -30$ nT, $3 < L < 5$ and outside MLT=3-9 are shown in this Figure. The blue and red lines with 25% and 75% quartiles represent the situation of -70 nT $< S_o < -30$ nT and $S_o < -70$ nT,

respectively. (a) Satellite cumulative time; (b) Sym-H; (c) IMF Bz; (d) AE index; (e) O⁺ pressure; (f) Total plasma pressure; (g) Pressure anisotropy; (h) \mathcal{R} value.

Figure 4. The temporal evolution of proton and oxygen pitch angle distributions as a function of time difference ($t=t_i - t_0$) between the observational point (t_i) and the universal time (t_0) of local sym-H minimum (S_o) in the time window of 12 hours before and 36 hours after the time t_0 . Only the data points of $\mathcal{R} > 0.35$ and $P_H > 0.5$ nPa and $P_O > 0.1$ nPa with $S_o < -30$ nT, $3 < L < 5$ and outside MLT=3-9 are shown in this Figure. (a-b) proton normalized flux at various energies under the situation of -70 nT $< S_o < -30$ nT and $S_o < -70$ nT, respectively; (c-d) oxygen normalized flux at various energies under the situation of -70 nT $< S_o < -30$ nT and $S_o < -70$ nT, respectively.

